J. Fluid Mech. (1992), *vol.* 237, *pp.* 395–411
Printed in Great Britain

Orbital flow around a circular cylinder. Part 1. Steady streaming in non-uniform conditions

By JOHN R. CHAPLIN

Ocean Engineering Research Centre, Department of Civil Engineering, City University, London EC1V 0HB, UK

(Received 8 May 1990 and in revised form 5 September 1991)

This work is concerned with the source of an important component of nonlinear loading on a horizontal cylinder beneath waves that is not present in conventional diffraction calculations. Earlier measurements (Chaplin 1984*b*) have suggested that circulation induced by steady streaming around the cylinder may be responsible for loading which in some cases reduces the perceived inertia force by 50%. The present work is aimed at studying the steady streaming around a cylinder in general non-uniform orbital flow, and determining whether in the particular case of wave-induced flow it could be related quantitatively to the loading.

The steady outer flow has been obtained numerically for cases where the steady streaming does not have a reversal, and for cases where a weak reversal is compatible with a uniform outer circulation. It is found that the outer circulation is closely related to the mean streaming velocity around the cylinder at the outer edge of the shear-wave layer. Results for conditions corresponding to previous measurements of force on a horizontal cylinder beneath waves suggest that separation, turbulence, transient effects and organized three-dimensional instabilities should also be considered.

1. Introduction

'Steady streaming' is the steady flow which is generated in an oscillatory boundary layer in conditions when the externally imposed flow over the boundary is oscillatory and non-uniform. Many theoretical and experimental investigations from Faraday (1831) and Rayleigh (1883) onwards have concentrated on the case of a cylinder forced to oscillate with small amplitude along a straight line normal to its axis. The non-uniformity of the boundary layer in this case is purely of the 'standing wave' type, since the motion around the cylinder differs in amplitude but not in phase. It is well known that the resulting steady streaming comprises a circulation in each quadrant of the fluid, with the fluid elements drawn towards that part of the boundary where the motion is tangential, and leaving the boundary where the motion is perpendicular. At these points the steady streaming at the outer edge of the boundary layer undergoes a reversal. Experimental and numerical solutions for this case are to be found, for example, in recent work by Kim & Troesch (1989), who also studied cases of steady streaming generated by rectilinear motion of cylinders of other cross-sections. Secondary flows generated by circular cylinders undergoing various two-dimensional oscillatory motions were considered by Kubo & Kitano (1980), Taneda (1980) and Kusukawa, Shimizu & Shinoda (1980). But in these cases also, the boundary layers were of the 'standing wave' type.

The case of a cylinder subject to orbital or stirring motion has on the other hand

received very little attention. Longuet-Higgins (1970) and Riley (1971) showed that for a circular cylinder executing a circular orbital motion in fluid initially at rest (or equivalently a stationary cylinder in uniform circular orbital flow), the streaming flow at infinite time takes the form of an irrotational vortex motion around the cylinder. In this case the non-uniformity of the boundary layer is of the 'progressive wave' type (since the motion changes only in phase around the cylinder), and the steady streaming at the outer edge of the boundary layer has no reversals.

The present work was stimulated by interest in the case of a horizontal cylinder beneath waves, aligned with its axis parallel to the wave crests. The limiting case of deep-water waves passing over a cylinder whose diameter is very small in comparison with the wavelength approaches that of uniform circular orbital flow. But in the general case, the ellipticity of the wave-induced orbital motion, and its non-uniformity over the cylinder's cross-section, ensure that the boundary layer has both standing and progressive wave features. When the motion is predominantly orbital, it is reasonable to expect that the steady streaming will be dominated by circulation around the cylinder. On the other hand when the waves are in shallower water and the orbital motion has small ellipticity, reversals in the streaming flow can be expected, as in the case of rectilinear motion. In this paper we are primarily concerned with the problem of predicting the circulation around the cylinder in the case where the ellipticity is sufficient to prevent reversals in the steady streaming; calculations described below permit the limiting condition to be identified.

Circulation generated by steady streaming around a cylinder in non-uniform conditions seems previously to have been studied only by Riley (1978). In that case, the non-uniformity arose not through the nature of the motion (which consisted as in Riley 1971 of uniform circular orbital flow), but from the elliptical cross-sectional shape of the cylinder. Riley computed two particular cases, cylinder ellipticities of 0.905 and 0.707, and found that in comparison with the case of a circular cylinder, the circulation strengths were increased respectively by about 3 and 39%. By analogy with the case of a horizontal circular cylinder beneath waves, it may be inferred that an increase in non-uniformity in the ambient flow, associated this time with the wave conditions, may similarly give rise to an increase in circulation strength.

Our interest in the circulation generated around a horizontal cylinder beneath waves stems from the possibility that it may have a significant effect on the force experienced by the cylinder. Experimental results (Chaplin, 1984*b*) suggest that the magnitude of the lift, generated by the combination of circulation and incident flow, may be as much as one-half of that of the load which can be attributed to the inviscid flow. This is potentially a matter of concern in the design of some buoyant offshore structures, where viscous effects are traditionally neglected.

Force measurements on a horizontal cylinder beneath waves (Chaplin 1984*b*), conducted in conditions where separation and vortex shedding are not likely to be important, showed that that part of the loading which could not be attributed to the inviscid flow increased in strength generally with the degree of non-uniformity of the ambient wave conditions. The purpose of the work described below is to determine whether such changes in the loading could be associated with changes in the strength of circulation around the cylinder, as suggested by Riley's computations for the non-circular cylinder. A companion paper (Chaplin 1992) describes a time-dependent Navier–Stokes solution aimed at the case of larger amplitude motions, for which the boundary-layer approach would not be appropriate.

Section 2 below applies Riley's (1971) approach to the problem of a circular

cylinder in more general orbital flow, and §3 describes the numerical solution for the outer circulation. Results presented in §4 for a horizontal cylinder beneath waves provide some support for the hypothesis that the viscous part of the loading may be associated with the calculated circulation strength, but show that other factors must also be significant.

2. Derivation of the stream function

The definition sketch figure 1 shows the cylinder (radius c) located at the origin of the polar coordinate system r, θ. At large distances from the cylinder the flow in the (r, θ)-plane conforms, in all respects but for an initially unknown circulation, to some given potential flow which is harmonic in time t with frequency ω, and which in the cylinder's absence would give rise (at $t = 0$) to a flow in the direction $\theta = 0$ of amplitude U at the origin. On the boundary of the cylinder the no-slip condition applies. It is assumed that the amplitude of the undisturbed motion at the cylinder is small in comparison with the radius, so that separation does not occur, and no wake is generated. The purpose of this section is to derive the most important parts of the stream function for the region surrounding the cylinder. The stream function ψ is related to the radial and tangential velocity components by

$$v_r = \frac{1}{r}\frac{\partial \psi}{\partial \theta}, \quad v_\theta = -\frac{\partial \psi}{\partial r}. \tag{2.1}$$

The structure of the solution and some of the equations will be found in Riley (1971, 1978) for the cases studied there, but are included below in a general form for a cylinder of circular cross-section.

At this point the problem is non-dimensionalized by normalizing time in terms of ω, lengths with respect to c, and velocities with respect to U. The vorticity transport equation then becomes

$$\frac{\partial(\nabla^2\psi)}{\partial t} - \frac{\epsilon}{r}\left\{\frac{\partial \psi}{\partial r}\frac{\partial(\nabla^2\psi)}{\partial \theta} - \frac{\partial \psi}{\partial \theta}\frac{\partial(\nabla^2\psi)}{\partial r}\right\} = \frac{\epsilon^2}{R_s}\nabla^4\psi, \tag{2.2}$$

where $\epsilon = U/\omega c$, $R_s = U^2/\omega\nu$. ϵ is related to the Keulegan–Carpenter number K_c used in the context of wave loading by $K_c = \pi\epsilon$, and R_s is a Reynolds number appropriate to the streaming flow. We follow Riley (1971) in adopting one double expansion for ψ in an inner region which accommodates the shear-wave layer, whose thickness is of order $\epsilon/R_s^{\frac{1}{2}}$, and another for the outer region. The outer asymptote of the inner stream function is made to match the inner asymptote of the outer stream function. The leading terms of the expansions are of the following form: for the outer region,

$$\psi = \psi_0 + \left(\frac{\epsilon^2}{R_s}\right)^{\frac{1}{2}}\psi_{01} + \ldots + \epsilon(\psi_{10}^{(s)} + \psi_{10}^{(u)}) + \epsilon^2\psi_2 + \epsilon^3\psi_3 + \ldots, \tag{2.3}$$

where the component stream functions are generally functions of r, θ and t, but (s) and (u) superscripts denote respectively the steady and time-dependent parts of ψ_{10}. The corresponding expansion

$$\Psi = \Psi_0 + \left(\frac{\epsilon^2}{R_s}\right)^{\frac{1}{2}}\Psi_{01} + \ldots + \epsilon(\Psi_{10}^{(s)} + \Psi_{10}^{(u)}) + \epsilon^2\Psi_2 + \epsilon^3\Psi_3 + \ldots \tag{2.4}$$

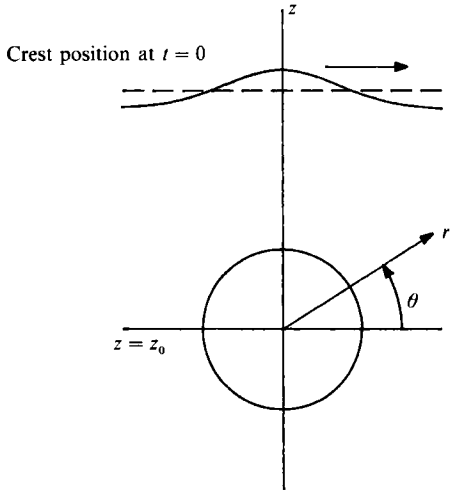

FIGURE 1. Definition sketch.

for the inner region makes use of the transformation

$$\Psi = \psi(R_s/2\epsilon^2)^{\frac{1}{2}}, \quad \rho = (r-1)\,(R_s/2\epsilon^2)^{\frac{1}{2}},$$

which leads to the requirement that at a given order and frequency the limiting value of $\partial\psi/\partial r$ as r tends to zero should equal the limiting value of $\partial\Psi/\partial\rho$ as ρ tends to infinity.

Substituting (2.3) and (2.4) into (2.2) and extracting terms of zeroth order yields

$$\frac{\partial}{\partial t}\nabla^2\psi_0 = 0, \tag{2.5}$$

$$\frac{\partial}{\partial t}\frac{\partial^2\Psi_0}{\partial\rho^2} = \frac{1}{2}\frac{\partial^4\Psi_0}{\partial\rho^4}. \tag{2.6}$$

Clearly ψ_0 is available as the irrotational solution to the inviscid flow problem, satisfying far-field conditions compatible with the specified ambient flow, and a slip condition (resolved by Ψ_0) at the cylinder's surface. It is assumed that ψ_0 is known in the form

$$\psi_0 = F(r,\theta)\,\mathrm{e}^{\mathrm{i}t}. \tag{2.7}$$

Here and below a complex expression denotes its real part. It may be shown that the general solution to (2.6), satisfying the matching requirement and the no-slip condition at the cylinder, is

$$\Psi_0 = [\rho + \tfrac{1}{2}(1-\mathrm{i})\,(\mathrm{e}^{-(1+\mathrm{i})\rho} - 1)]f(\theta)\,\mathrm{e}^{\mathrm{i}t}, \tag{2.8}$$

where

$$f(\theta) = \left.\frac{\partial F}{\partial r}\right|_{r=1}. \tag{2.9}$$

Extracting next from the expansion of (2.2) terms of order $(\epsilon^2/R_s)^{\frac{1}{2}}$ leads to

$$\frac{\partial}{\partial t}\nabla^2\psi_{01} = 0, \tag{2.10}$$

and
$$\frac{1}{2}\frac{\partial^4 \Psi_{01}}{\partial \rho^4} - \frac{\partial^3 \Psi_{01}}{\partial t\, \partial \rho^2} = \sqrt{2}\left(\frac{\partial^2 \Psi_0}{\partial t\, \partial \rho} - \frac{\partial^3 \Psi_0}{\partial \rho^3}\right). \tag{2.11}$$

Particular solutions for ψ_{01} and Ψ_{01} are given by Riley (1971). They are not developed in the present case since terms of this order are unlikely to be significant in the context of high-Reynolds-number flows.

At order ϵ the unsteady terms in the expansion of (2.2) are given by

$$\frac{\partial}{\partial t}(\nabla^2 \psi_{10}^{(u)}) = 0, \tag{2.12}$$

$$\frac{1}{2}\frac{\partial^4 \Psi_{10}^{(u)}}{\partial \rho^4} - \frac{\partial}{\partial t}\frac{\partial^2 \Psi_{10}^{(u)}}{\partial \rho^2} = \left[\frac{\partial \Psi_0}{\partial \theta}\frac{\partial^3 \Psi_0}{\partial \rho^3} - \frac{\partial \Psi_0}{\partial \rho}\frac{\partial^3 \Psi_0}{\partial \theta\, \partial \rho^2}\right]^{(u)} \tag{2.13}$$

$$= -\mathrm{i}\rho\, \mathrm{e}^{-(1+\mathrm{i})\rho} f(\theta) f'(\theta) \mathrm{e}^{2\mathrm{i}t}, \tag{2.14}$$

evaluating the right-hand side of (2.13) from (2.8); the prime denotes differentiation with respect to θ. Solutions for $\psi_{10}^{(u)}$ and $\Psi_{10}^{(u)}$ compatible with the boundary conditions are

$$\psi_{10}^{(u)} = 0, \tag{2.15}$$

$$\Psi_{10}^{(u)} = \frac{1}{4\mathrm{i}}\left\{2\rho \mathrm{e}^{-(1+\mathrm{i})\rho} + \frac{1-\mathrm{i}}{\sqrt{2}}\mathrm{e}^{-\sqrt{2}(1+\mathrm{i})\rho} - \frac{1-\mathrm{i}}{\sqrt{2}}\right\} f(\theta) f'(\theta) \mathrm{e}^{2\mathrm{i}t}. \tag{2.16}$$

For the steady part of the stream function at order ϵ, (2.2) gives

$$\frac{1}{2}\frac{\partial^4 \Psi_{10}^{(s)}}{\partial \rho^4} = \left[\frac{\partial \Psi_0}{\partial \theta}\frac{\partial^3 \Psi_0}{\partial \rho^3} - \frac{\partial \Psi_0}{\partial \rho}\frac{\partial^3 \Psi_0}{\partial \theta\, \partial \rho^2}\right]^{(s)} \tag{2.17}$$

$$= [-\mathrm{i}\rho \mathrm{e}^{-(1+\mathrm{i})\rho} + (1-\mathrm{i})(\mathrm{e}^{-2\rho} - \mathrm{e}^{-\rho}\cos\rho)]\, f(\theta)\, \overline{f'(\theta)} \tag{2.18}$$

for the inner region, where the overbar denotes the complex conjugate. Integrating (2.18) and using the boundary conditions that $\partial \Psi_{10}^{(s)}/\partial \rho$ must remain bounded as $\rho \to \infty$, and $\partial \Psi_{10}^{(s)}/\partial \rho = \Psi_{10}^{(s)} = 0$ on $\rho = 0$, gives

$$\Psi_{10}^{(s)} = \{(1+\mathrm{i})\mathrm{e}^{-(1+\mathrm{i})\rho} + \tfrac{1}{2}\mathrm{i}\rho\, \mathrm{e}^{-(1+\mathrm{i})\rho} + \tfrac{1}{8}(1-\mathrm{i})\mathrm{e}^{-2\rho} + \tfrac{1}{2}(1-\mathrm{i})\mathrm{e}^{-\rho}\cos\rho$$
$$+ \tfrac{3}{4}(1+\mathrm{i})\rho - \tfrac{1}{8}(13+3\mathrm{i})\}\, f(\theta)\, \overline{f'(\theta)}. \tag{2.19}$$

$\Psi_{10}^{(s)}$ is the stream function of the steady streaming, which at the outer edge of the shear-wave layer gives rise to a steady clockwise tangential velocity represented in dimensionless terms by

$$U_s = \tfrac{3}{4}(1+\mathrm{i})\, f(\theta)\, \overline{f'(\theta)}. \tag{2.20}$$

For the case of a circular cylinder in uniform clockwise circular orbital flow, $f(\theta) = -2\mathrm{i}c^{\mathrm{i}\theta}$, and $U_s = 3$. The outer flow $\psi_{10}^{(s)}$ in this case is a clockwise potential vortex (as mentioned above), whose dimensionless circulation $\Gamma_0 = 6\pi$ will be used later for reference purposes.

It is $\psi_{10}^{(s)}$ that is our chief concern, since it is the first term that is likely to give rise to significant viscosity-induced loading at high Reynolds numbers; the induced circulation (whose magnitude is the same for all non-zero values of viscosity) can be expected to generate lift through the Magnus effect.

Terms in the outer expansion of (2.2) at orders ϵ^2 and ϵ^3 provide respectively

$$\frac{\partial}{\partial t}\nabla^2\psi_2-\frac{1}{r}\left\{\frac{\partial\psi_0}{\partial r}\frac{\partial\nabla^2\psi_{10}^{(s)}}{\partial\theta}-\frac{\partial\psi_0}{\partial\theta}\frac{\partial\nabla^2\psi_{10}^{(s)}}{\partial r}\right\}=0, \tag{2.21}$$

$$\frac{1}{R_s}\nabla^{4'}\psi_{10}^{(s)}+\frac{1}{r}\left\{\frac{\partial\psi_{10}^{(s)}}{\partial r}\frac{\partial\nabla^2\psi_{10}^{(s)}}{\partial\theta}-\frac{\partial\psi_{10}^{(s)}}{\partial\theta}\frac{\partial\nabla^2\psi_{10}^{(s)}}{\partial r}\right\}=-\frac{1}{r}\left\{\frac{\partial\psi_0}{\partial r}\frac{\partial\nabla^2\psi_2}{\partial\theta}-\frac{\partial\psi_0}{\partial\theta}\frac{\partial\nabla^2\psi_2}{\partial r}\right\}^{(s)}. \tag{2.22}$$

For the uniform orbital flow case

$$\nabla^2\psi_{10}^{(s)}=0 \tag{2.23}$$

satisfies both (2.22) and the inner boundary condition of a steady streaming flow U_s which is the same at all points around the cylinder. For non-uniform cases, Riley (1978) argued that the form of (2.22) points to the existence of an outer layer whose thickness is of order $R_s^{\frac{1}{2}}$. This layer accommodates the transition between the outer region in which $\psi_{10}^{(s)}$ satisfies (2.23), and the outer limit of the shear-wave layer where $\partial\psi_{10}^{(s)}/\partial r$ must match U_s.

For the non-uniform flow case, $\psi_{10}^{(s)}$ in the outer layer can be found as described in the next section through numerical integration of a boundary-layer version of (2.22). First it is necessary to express the right-hand side of (2.22) in terms of the known zeroth-order flow $F(r,\theta)$. The terms in $\nabla^2\psi_2$ can be replaced by integrating (2.21) with respect to t, and differentiating with respect to θ and r. Equation (2.22) then becomes

$$\frac{1}{R_s}\nabla^4\psi_{10}^{(s)}+\frac{1}{r}\left\{\frac{\partial\psi_{10}^{(s)}}{\partial r}\frac{\partial\nabla^2\psi_{10}^{(s)}}{\partial\theta}-\frac{\partial\psi_{10}^{(s)}}{\partial\theta}\frac{\partial\nabla^2\psi_{10}^{(s)}}{\partial r}\right\}=-\frac{\mathrm{i}}{2}\frac{\partial F}{\partial r}\frac{1}{r}\frac{\partial}{\partial\theta}\left(\frac{\partial\bar{F}}{\partial r}\right)\frac{1}{r}\frac{\partial\nabla^2\psi_{10}^{(s)}}{\partial\theta}. \tag{2.24}$$

A boundary-layer approximation to (2.24) leads to

$$\frac{1}{R_s}\frac{\partial^4\psi_{10}^{(s)}}{\partial r^4}+\frac{\partial\psi_{10}^{(s)}}{\partial r}\frac{1}{r}\frac{\partial^3\psi_{10}^{(s)}}{\partial\theta\,\partial r^2}-\frac{1}{r}\frac{\partial\psi_{10}^{(s)}}{\partial\theta}\frac{\partial^3\psi_{10}^{(s)}}{\partial r^3}=-\frac{\mathrm{i}}{2}\frac{\partial F}{\partial r}\frac{1}{r}\frac{\partial}{\partial\theta}\left(\frac{\partial\bar{F}}{\partial r}\right)\frac{1}{r}\frac{\partial^3\psi_{10}^{(s)}}{\partial\theta\,\partial r^2}. \tag{2.25}$$

Using next the transformation

$$r-1=y/R_s^{\frac{1}{2}};\quad \psi_{10}^{(s)}=\phi/R_s^{\frac{1}{2}};\quad \frac{1}{r}\frac{\partial}{\partial\theta}=-\frac{\partial}{\partial x}, \tag{2.26}$$

integrating (2.25) with respect to y and putting $u=\partial\phi/\partial y$, $-v=\partial\phi/\partial x$ leads to the boundary-layer equation

$$-\frac{\partial^2 u}{\partial y^2}+u\frac{\partial u}{\partial x}+v\frac{\partial u}{\partial y}=R\frac{\partial u}{\partial x}, \tag{2.27}$$

where

$$R=-\tfrac{1}{2}\mathrm{i}f(\theta)\,\overline{f'(\theta)}. \tag{2.28}$$

Equation (2.27) is to be compared with equation (29*b*) of Riley (1978). In the limit $y=0$, u must match U_s, the dimensionless steady streaming at the outer edge of the shear-wave layer, known from (2.20). As $y\to\infty$ on the other hand, u must tend at infinite time towards a flow associated with a potential vortex motion around the cylinder. The strength of the circulation around the cylinder Γ is at this stage unknown but must be determined by use of the boundary condition

$$\frac{\partial u}{\partial y}\to 0,\quad y\to\infty. \tag{2.29}$$

As described below, it is found that this condition can be satisfied for just one outer limiting value of u, denoted U_1'. In the case of a non-circular cylinder (Riley 1978), U_1' must vary around the circumference of the cylinder in order to accommodate the distribution of the potential flow associated with given circulation. In the present case however U_1' is not a function of x, so that in an unbounded fluid

$$u \to U_1' = \frac{\Gamma}{2\pi} \quad \text{as} \quad y \to \infty. \tag{2.30}$$

3. The numerical solution

Equation (2.27) was solved for $u(x, y)$ using a simple numerical scheme similar to that proposed by Riley. The method proceeds in the x-direction in a step-by-step fashion to obtain by finite differences an approximate solution to (2.27) expressed in the form

$$-\frac{\partial^2 u}{\partial y^2} + u\frac{\partial u}{\partial x} - \frac{\partial \phi}{\partial x}\frac{\partial u}{\partial y} - R\frac{\partial u}{\partial x} = 0. \tag{3.1}$$

Adopting the notation $u(x = i\,\delta x, y = j\,\delta y) = u_{i,j}$, (3.1) may be approximated using central differences at the point $(i-\frac{1}{2}, j)$ as

$$-\frac{u_{i-\frac{1}{2},j+1} - 2u_{i-\frac{1}{2},j} + u_{i-\frac{1}{2},j-1}}{\delta y^2} + u^*_{i-\frac{1}{2},j}\frac{u_{i,j} - u_{i-1,j}}{\delta x}$$

$$-\frac{\phi^*_{i,j} - \phi_{i-1,j}}{\delta x}\frac{u_{i-\frac{1}{2},j+1} - u_{i-\frac{1}{2},j-1}}{2\delta y} - R_{i-\frac{1}{2}}\frac{u_{i,j} - u_{i-1,j}}{\delta x} = 0 \tag{3.2}$$

where $u_{i-\frac{1}{2},j} = \frac{1}{2}(u_{i,j} + u_{i-1,j})$, etc.

In advancing from station $i-1$ to i, equation (3.2) is solved iteratively for the $u_{i,j}$ with ϕ updated after each iteration by the trapezoidal rule,

$$\phi_{i,0} = 0, \quad \phi_{i,j} = \phi_{i,j-1} + \tfrac{1}{2}(u_{i,j-1} + u_{i,j})\,\delta y, \quad j = 1, 2 \ldots J. \tag{3.3}$$

Note that (3.2) has been linearized by using lagged parameters in the second and third terms; the superscript * denotes a value from the preceding iteration. On this basis (3.2) forms a tri-diagonal system for the unknowns $u_{i,j}$ and can be formulated to incorporate the boundary conditions $u_{i,0} = U_s$, $u_{i,j} = U_1$, both treated as known constants. Because of the presence of the nonlinear terms, and the need to compute ϕ between iterations, the tri-diagonal system must be solved repeatedly at each step until convergence is achieved.

The solution is started with assumed values for $u_{0,j}$, and marches in the x-direction around the cylinder repeatedly until insignificant changes are detected from one circuit to the next. The rate of convergence of the solution was improved by using an over-relaxation factor of 1.2 on $u_{0,j}$ at the end of each circuit. For a given ambient flow, convergence in this respect may be obtained with any chosen value of U_1; but with an arbitrary choice of U_1 the condition (2.29) would not in general be satisfied anywhere. It was found however that as U_1 approached one particular value, say U_1', $\partial u/\partial y$ at the outer edge of the domain ($y = J\,\delta y$) would tend towards zero *at all values of* x simultaneously. The value of U_1' was found by solving $g(U_1) = 0$ by bisection, where $g(U_1)$ represents the converged mean value over x of $\partial u/\partial y$ at $y = J\,\delta y$, computed with a particular value of U_1. The function g is plotted in figure 2

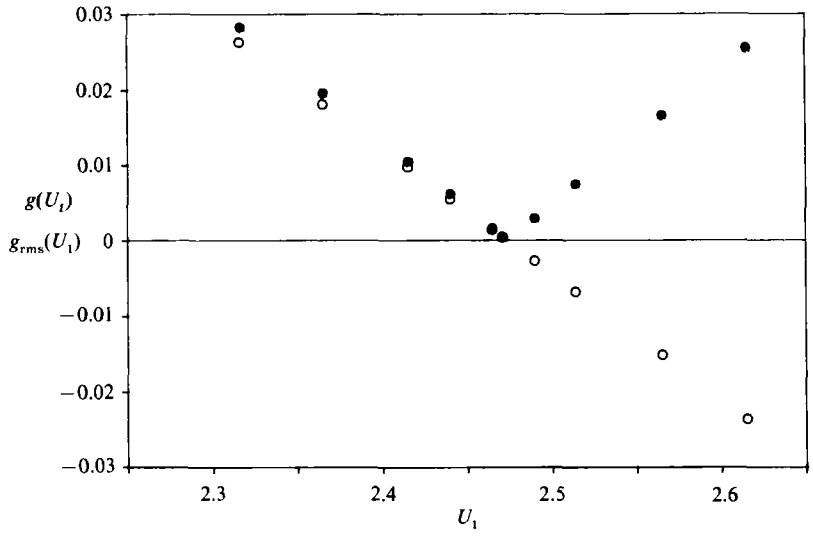

FIGURE 2. The mean (○) and root-mean-square (●) values of $\partial u/\partial y$ around the circumference at the outer edge of the computational domain, as functions of the velocity, U_1 imposed at the boundary. Wave-induced non-uniform flow (case II as defined in §4) with $kc = 0.3$ and ellipticity 0.7.

in the region of the solution for a particular case, together with g_{rms}, the root-mean-square value, over x, of $\partial u/\partial y$ at $y = J\,\delta y$. The fact that g crosses zero at a point where the root-mean-square value is also very close to zero suggests that for this value of U_1 the streaming velocity satisfies (2.29) everywhere, to within the accuracy of the computation.

It was assumed that U_1' represented the naturally occurring case at infinite time, and that the circulation established around the cylinder would be the corresponding value of $\Gamma = 2\pi U_1'$; a dimensional circulation of $2\pi UecU_1'$. The cases presented below (and in figure 2) were computed with $\delta x = \pi/100$, $\delta y = 0.06$, and $J\,\delta y = 12$ (i.e. 200 points in each direction). Convergence tests showed that the effect of doubling δx or δy or of halving $J\,\delta y$ was a change in the computed circulation of no more than 1.2%, and generally much less than this. The convergence criterion required that the maximum change in u at any point from one circuit to the next should be less than 1.0×10^{-5}. Computations were carried out on a SUN SPARC station 1, with a typical run-time of 6 min for each case.

4. Calculation of circulation strength for particular cases

Numerical results for a circular cylinder in orbital flow are presented below for the following cases:

Case I. A stationary cylinder in uniform elliptical orbital flow

For uniform elliptical orbital flow in the clockwise direction (equivalent to a cylinder moving around an elliptical path in initially still fluid),

$$f(\theta)\,\overline{f'(\theta)} = 4[(1-E^2)\sin\theta\cos\theta - \mathrm{i}E],$$

where E is the ellipticity of the motion. The streaming flow is given by

$$U_s = 3[(1-E^2)\sin x\cos x + E], \tag{4.1}$$

where x is measured from $\theta = \frac{1}{2}\pi$, i.e. clockwise from the top of the cylinder. From (4.1) it may be inferred that for ellipticities above $\sqrt{2}-1$, the streaming flow will have no reversal.

Case II. A stationary cylinder in wave-induced orbital flow

If a cylinder beneath waves is submerged by more than about 5 radii, the effect of the cylinder on the waves in most respects may be neglected, and the ambient flow in its vicinity can be approximated by using the circle theorem (Ogilvie 1963; Chaplin 1981). In this case,

$$f(\theta)\,\overline{f'(\theta)} = \frac{2}{\cosh^2 ks}\{kc\sinh 2A\cos\theta + \sin 2\theta + \mathrm{i}[kc\sin 3\theta - kc\cosh 2A\sin\theta - \sinh 2A]\}, \tag{4.2}$$

where $A = ks + kc\sin\theta$, the wavelength is $2\pi/k$, and s is the elevation of the cylinder above the sea bed. The ellipticity $E = \tanh ks$.

Case III. A stationary cylinder beneath waves

For the case of a horizontal cylinder submerged beneath waves which are propagating in the positive x-direction in deep water, the potential F (including the effect of the cylinder on the free surface) may be found from Ogilvie (1963). It follows that

$$f(\theta)\,\overline{f'(\theta)} = \frac{4\mathrm{i}}{(kc)^2(1+S_\epsilon^2)}\left(\sum_{m=1}^{M}\frac{m\epsilon_m\,\mathrm{e}^{\mathrm{i}m\theta}}{(\mathrm{i}kc)^m}\right)\left(\sum_{m=1}^{M}\frac{m^2\epsilon_m\,\mathrm{e}^{-\mathrm{i}m\theta}}{(-\mathrm{i}kc)^m}\right), \tag{4.3}$$

where ϵ_m $(m = 1, 2, \ldots, M)$ and S_ϵ are defined in terms of kc and the cylinder's elevation z_0 with respect to mean water level, as in Ogilvie (1963). The ellipticity is unity.

In cases II and III the fluid is not unbounded. In view of (2.30), the present approach can therefore be applied to these flows only on the basis that we neglect all effects of the fluid boundaries at the free surface and at the bed on the viscosity-induced flow. In instances when the cylinder is close to the surface or to the bed this simplification may profoundly affect the results, but cases II and III are included here since they can provide an indication of the effects of another essential feature of flow induced by waves, namely its non-uniformity.

The distribution of U_s around the cylinder for each type of ambient orbital flow is shown in figure 3. In uniform orbital flow (figure 3*a*) the steady streaming has equal maxima at $\theta = \frac{1}{4}\pi$ and $\frac{5}{4}\pi$. Figure 3(*b*) shows that the distortion associated with finite wavelength is considerable for a value of kc as low as 0.05 (a wavelength-to-diameter ratio of about 1/63), and that the steady streaming is much increased over the top of the cylinder as its submergence is reduced. A more extreme case is that of $kc = 0.6$ (figure 3*c*), where the steady streaming at the highest part of the cylinder's cross-section is as much as 100 times that at the lowest part.

Since the outer circulation is driven by the steady streaming, it seems reasonable to relate its strength Γ to the mean value $\bar{U}_s$ of the streaming velocity around the cylinder's circumference. $\bar{U}_s$ is influenced both by the ellipticity of the flow and by the degree of its non-uniformity. In uniform flow, $\bar{U}_s$ increases in proportion to the ellipticity, and figure 4 shows that it also increases rapidly with kc when the effect of the cylinder on the waves is neglected. The effect of the proximity of the free surface is generally to increase the mean streaming flow still further, as shown in figure 5.

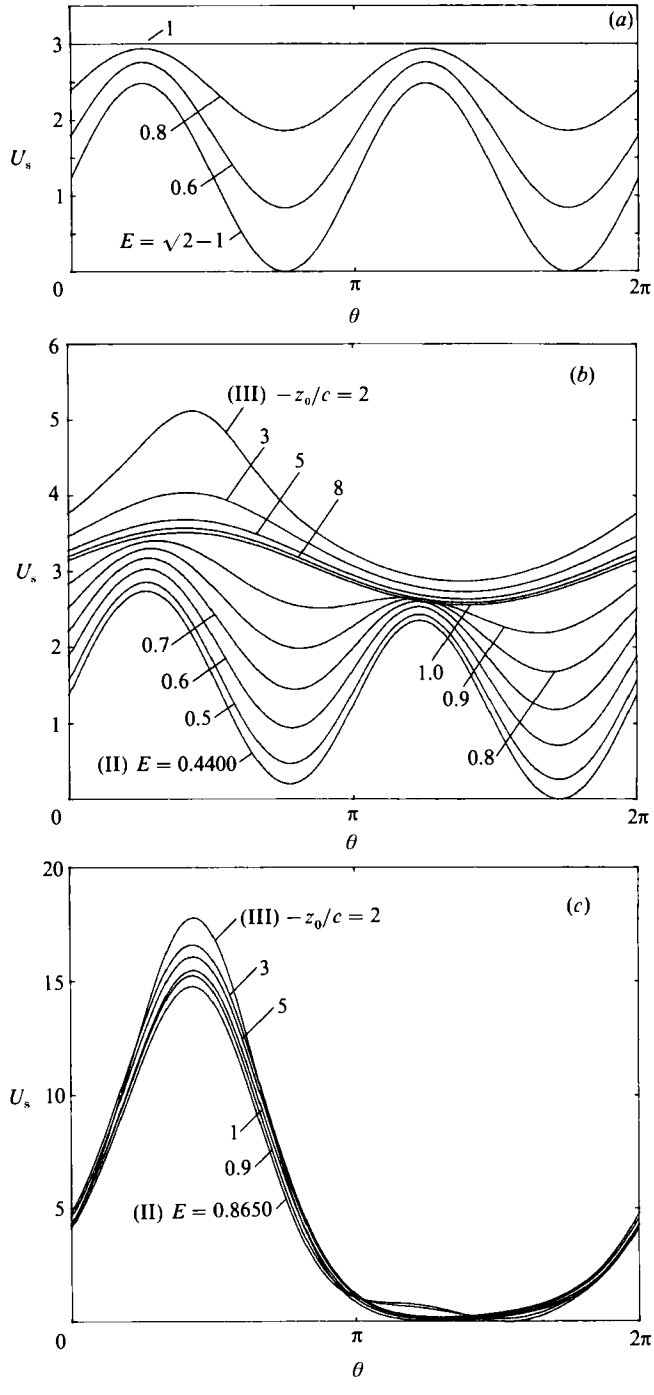

FIGURE 3. Distribution of streaming flow around a circular cylinder. (*a*) Case I: uniform elliptical orbital flow. (*b*) $kc = 0.05$. Case II: Wave-induced flow without surface interaction, various ellipticities; case III: wave-induced flow with surface interaction, various submergences. (*c*) As (*b*) but for $kc = 0.6$.

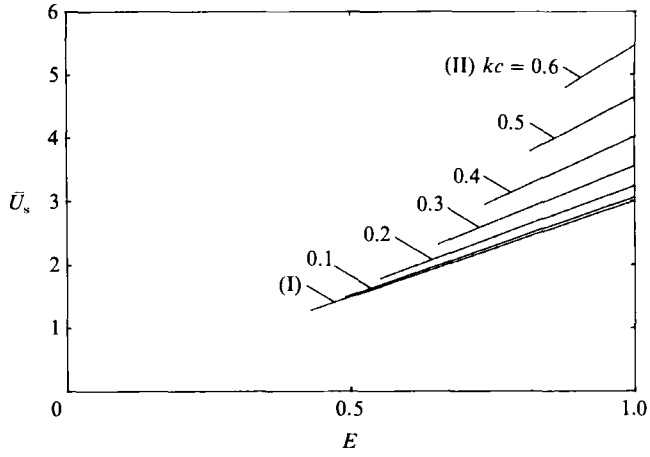

FIGURE 4. Mean streaming flow around the cylinder's circumference for conditions in which there is no reversal. Case I and case II at various values of kc.

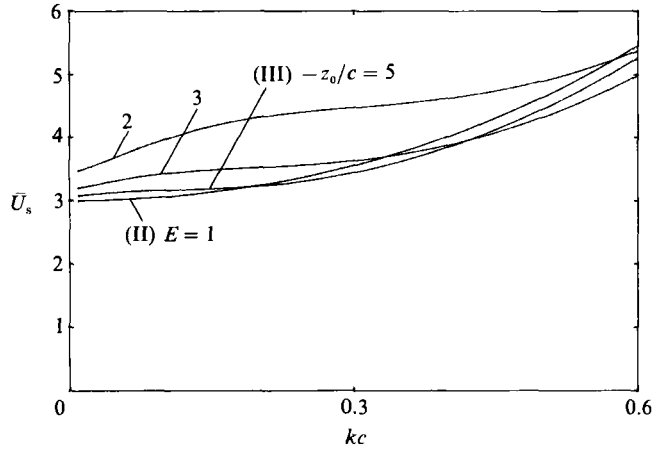

FIGURE 5. As for figure 4; case II for circular orbital flow, and case III for various submergences.

Computed outer circulation strengths are plotted in figure 6 for uniform and wave-induced flows, as a function of E for various values of kc. For each case, the symbol on the line identifies the ellipticity at which the minimum steady streaming U_s at the outer edge of the shear-wave layer reaches zero. For ellipticities smaller than this, the steady streaming reverses over a small region of the cylinder's surface, though the existence of a solution indicates that there is no reversal in the outer flow. Ultimately, for still smaller ellipticities, the tri-diagonal system (3.2) failed to converge. It was found that in each case the limiting ellipticity at which this happened (where the line in figure 6 is terminated) corresponded closely to that at which the minimum value of $U_s - R$ reached zero.

Though numerical difficulties might have been expected, solutions with reversed steady streaming were obtained without the use of any special techniques. But it should be noted that the marching solution carries forward information from all points around the cylinder, so that in the region of recirculation the computed flow is influenced by the motion both upstream and downstream. In the converged

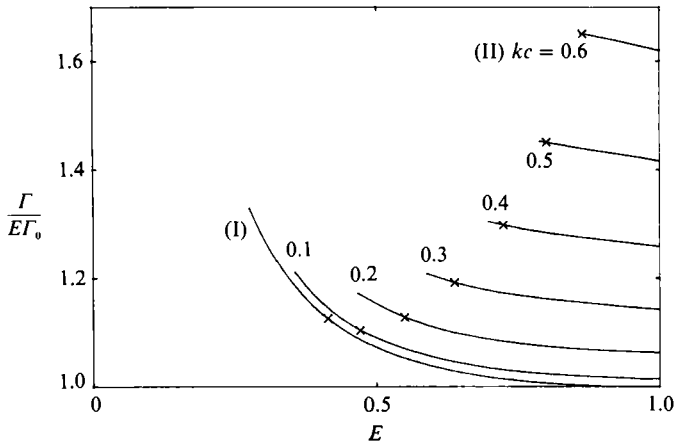

FIGURE 6. Outer circulation as a function of ellipticity; case I and case II at various values of kc. The symbol on the line for each case identifies the minimum ellipticity for which there is no reversal in the steady streaming.

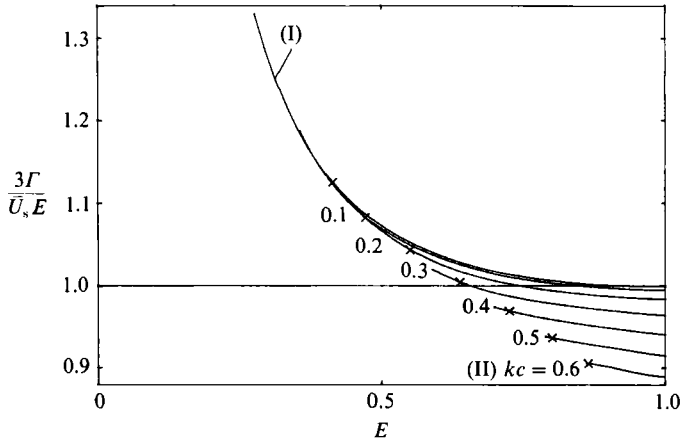

FIGURE 7. Outer circulation referred to the mean steady streaming velocity; case I and case II at various values of kc.

solution the finite-difference equations were satisfied at all points around the cylinder's circumference. It may be concluded that the occurrence of reversed steady streaming does not lead immediately to a major reorganization of the flow, but that the recirculation is at first contained within the thickness of the boundary layer. A related case was solved by Wang & Shen (1978) with a similar marching technique, which was found to pass without difficulty through a confined region of reversed flow. However, if the strength of the reversed flow is increased (in the present case by a decrease in ellipticity), a numerical breakdown can be expected where the flow begins ultimately to break away from the surface.

The influence of the degree of non-uniformity in the flow on the circulation is largely through its effect on the mean streaming velocity $\bar{U}_s$ at the outer edge of the shear-wave layer. Figure 7 shows that when the circulation strength is normalized with $\bar{U}_s$ it does not depart far from that obtained in uniform orbital elliptical flow.

Corresponding results for the case when the cylinder is close to the surface are given in figures 8 and 9. At the lower values of kc, the absolute circulation strength

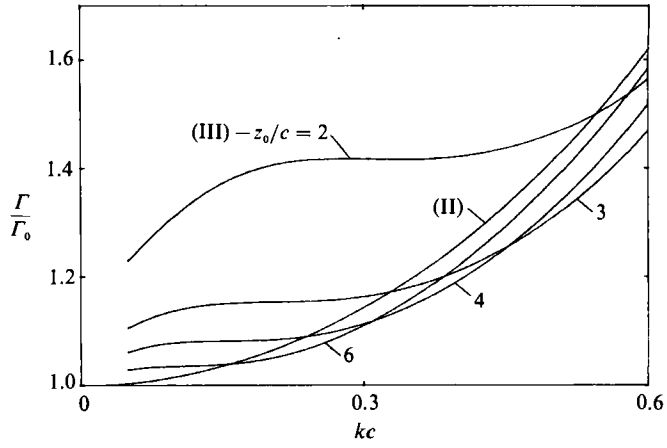

FIGURE 8. As for figure 6; case II at $E = 1$; case III for various submergences.

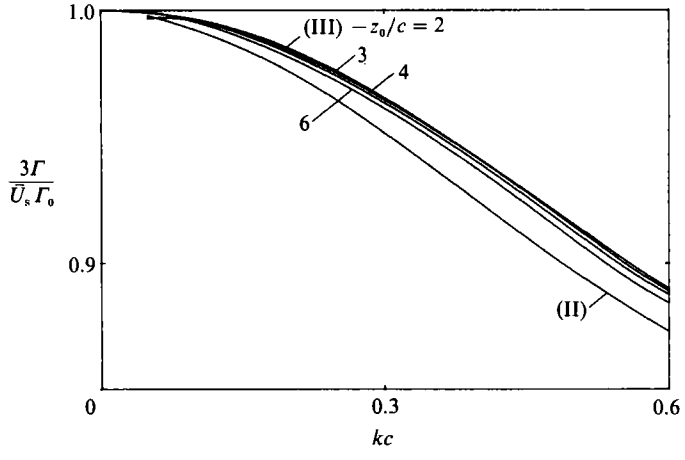

FIGURE 9. As for figure 7; case II at $E = 1$; case III for various submergences.

increases rapidly as the submergence is decreased, but figure 9 shows that this can be attributed almost entirely to the changes in mean circulation $\bar{U}_s$.

5. Experimental comparisons

In the absence of velocity measurements from which circulation strengths could be obtained, we make comparisons between computed circulations and those which may be inferred from measurements of the force on a horizontal cylinder beneath waves (Chaplin 1984*b*). In the analysis of these experiments, the magnitudes of the x- and y-components of the force per unit length on the cylinder at a frequency of n times the wave frequency ω were expressed as

$$F_x^{(n)} = \sum_m C_{xnm} \rho c^3 \omega^2 K_c^m; \quad F_y^{(n)} = \sum_m C_{ynm} \rho c^3 \omega^2 K_c^m. \tag{5.1}$$

The results revealed a strong nonlinear force in the terms C_{x13} and C_{y13} which may be interpreted as the Kutta–Joukowski lift arising from circulation around the cylinder. In the Appendix it is shown that in unsteady non-uniform inviscid flow the lift is

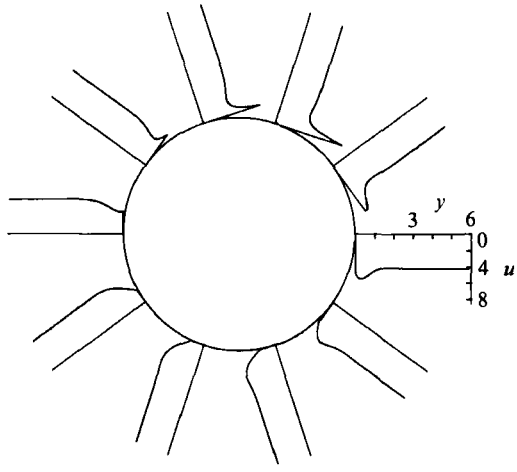

FIGURE 10. Steady streaming velocity distributions for the conditions of case E in table 1.

Case	z_0/c	kc	Γ_e	Γ
B	−5	0.206	6.5	20.0
C	−3	0.206	11.2	21.7
D	−3	0.365	11.2	22.3
E	−2	0.206	18.0	26.5
F	−2	0.365	19.5	26.6
G	−2	0.570	40.3	28.5

TABLE 1. Circulations inferred from force measurements (Chaplin 1984*b*) compared with those computed using the method of §3

proportional to the product of the circulation and the speed of the instantaneous undisturbed flow at the location of the cylinder's axis. On this basis the force coefficients C_{x13} and C_{y13} would be associated with circulation Γ_e, where

$$C_{x13} = C_{y13} = -\Gamma_e/\pi^3. \tag{5.2}$$

A formal determination of C_{x13} and C_{y13} would require the evaluation of terms in the stream function at higher orders than any obtained in §2. However, it is clear that if the circulation outside a thin layer surrounding the cylinder were uniform, it would generate a force whose magnitude would be represented approximately by (5.2). Forces on the cylinder also arise through the direct effect of viscosity on normal and shear stresses around its circumference. These were given in Chaplin (1984*b*) and shown to be insignificant at the Reynolds numbers at which the experiments were carried out.

For each experimental case, Table 1 compares Γ_e with Γ, the circulation computed for the appropriate conditions using the method described in §3.

The computed distribution of streaming flow in the outer layer around the cylinder is plotted for case E in figure 10. This is a case in which there is rather strong non-uniformity of the ambient flow across the cylinder's diameter, as shown by the large difference between the strength of steady streaming below and above the cross-section. Across the outer layer this non-uniformity is smoothed out in accordance with (2.27), to offer to the ambient flow a uniform steady flow which matches that due to a potential vortex centred on the cylinder. An indication of the strength of the

flow shown in figure 10 is conveyed by the fact that when the Keulegan–Carpenter number is around 0.5, the induced velocity is of a magnitude similar to that of the wave-induced ambient flow.

The quantitative agreement between inferred and computed circulations in table 1 is not good, and probably the most significant result is that in both cases there is an increase in strength as the submergence of the cylinder is decreased. As demonstrated above, this can be attributed mainly to the increase in steady streaming over the top of the cylinder.

In the absence of more detailed experimental results, we speculate that the poor agreement shown in table 1 may be associated with the following factors:

(i) *Organized three-dimensional instabilities.* In the case of rectilinear harmonic motion, the two-dimensional flow is disrupted at low values of the Reynolds number-to-Keulegan–Carpenter number ratio by the 'Honji instability' (Honji 1981; Sarpkaya 1986). It is likely that in a modified form the same mechanism affects the generation of steady streaming around a cylinder in orbital flow.

(ii) *The rate of spread of the circulation.* The outer flow at radius r becomes steady only after a time of order $(r-c)^2/\nu$ (Longuet-Higgins 1970). The force measurements to which we refer were completed after about 16 waves had passed the cylinder from the front of the wave train (Chaplin 1984*b*). Though no systematic change was detected over the preceding eight waves, the subsequent convergence to the conditions at infinite time, as represented in the boundary-layer calculations, may be so slow that it is dominated by other factors, such as mass transport generated by the waves.

(iii) *Separation.* The boundary-layer approach also neglects the possibility of separation, which would probably influence the outer circulation and the loading. Earlier visualizations (Chaplin 1984*a*) did not however reveal any large-scale flow structures in the Keulegan–Carpenter number range for which there is a clearly defined reduction in loading, apparently due to circulation.

(iv) *Turbulence.* Evidence from measurements in planar oscillatory flow (Sarpkaya 1986) suggests that boundary-layer turbulence may have occurred in some of the experiments quoted above. Very little is known about steady streaming in turbulent conditions, though the results of experiments in waves at Reynolds numbers around 200000 (Chaplin 1988) showed similar reductions in the perceived inertia force. At a given Keulegan–Carpenter number the effect was weaker, though it persisted over a much greater range. These observations suggest that the process can be significantly affected by boundary-layer turbulence.

6. Conclusions

The steady circulation around a cylinder in orbital flow is predominantly related to the mean streaming velocity at the outer edge of the shear-wave layer. The nature of the ambient flow has a weaker effect. In uniform elliptical orbital flow the circulation increases as the ellipticity of the flow is reduced from unity; in wave-induced flows, it decreases as the wavelength or the submergence is increased. Results computed for uniform elliptical orbital flow include cases where a reversal in the steady streaming at the outer edge of the shear-wave layer is found to be compatible with a uniform outer circulation. This computation broke down, however, at an ellipticity of about 0.277.

Computed circulation strengths do not relate well to the nonlinear features of previously measured forces on a horizontal cylinder beneath waves, though there is

some similarity with respect to the changes that occur in both cases with cylinder submergence. In trying to explain the discrepancies, further attention should be given to organized three-dimensional instability, the time-dependent growth of the circulation, separation, and turbulence.

This work was funded by the Department of Energy, as part of the Managed Programme of Research into Floating Production Systems. The Programme is supported also by the Science and Engineering Research Council and by fourteen industrial subscribers. The author acknowledges the benefit of discussions with Professor Norman Riley.

Appendix. Kutta–Joukowski lift in unsteady non-uniform flow

The purpose of this appendix is to show that the well-known result for the lift on a cylinder in a steady stream with circulation applies also in the case of unsteady non-uniform ambient flow.

Let $f(z)$ represent the complex potential of an irrotational two-dimensional unsteady inviscid flow, whose singularities are all at a distance greater than c from the origin. On introducing into the flow a circular cylinder of radius c at the origin, and a steady circulation Γ around it, the complex potential becomes

$$w = f(z) + \bar{f}\left(\frac{c^2}{z}\right) - \frac{\mathrm{i}\Gamma}{2\pi}\ln z. \tag{A 1}$$

using the circle theorem (see Milne-Thomson 1968). By Blasius's theorem (extended by Milne-Thomson) the x- and y-components of force per unit length on the cylinder are given by

$$X - \mathrm{i}Y = \tfrac{1}{2}\mathrm{i}\rho \oint \left(\frac{\mathrm{d}w}{\mathrm{d}z}\right)^2 \mathrm{d}z - \mathrm{i}\rho \frac{\partial}{\partial t}\oint \bar{w}\,\mathrm{d}\bar{z}, \tag{A 2}$$

where the integrations are to be taken around the cylinder, or around any larger contour which does not introduce any singularities. Evaluating (A 2) by the residue theorem, we look for terms involving z^{-1} in the expansion of the right-hand side. In the region of the cylinder $f(z)$ must be expressible in the form

$$f(z) = a_0 + a_1 z + a_2 z^2 + \ldots. \tag{A 3}$$

Therefore, on substituting (A 1) into (A 2), the part which involves Γ is simply $\mathrm{i}\rho\Gamma a_1$. This leads to the result that the effect of the circulation is a force of magnitude $\rho V\Gamma$ per unit length, where $V = |a_1|$, the speed of the instantaneous undisturbed flow at the location of the axis of the cylinder. The direction of the force is normal to this flow.

REFERENCES

CHAPLIN, J. R. 1981 On the irrotational flow around a horizontal cylinder in waves. *Trans. ASME* E: *J. Appl. Mech.* **48**, 689–694.

CHAPLIN, J. R. 1984*a* Mass transport around a horizontal cylinder beneath waves. *J. Fluid Mech.* **140**, 175–187.

CHAPLIN, J. R. 1984*b* Forces on a horizontal cylinder beneath waves. *J. Fluid Mech.* **147**, 449–464.

CHAPLIN, J. R. 1988 Non-linear forces on horizontal cylinders in the inertia regime in waves at high Reynolds numbers. *Proc. Intl BOSS Conf, Trondheim*, pp. 505–518.

CHAPLIN, J. R. 1992 Orbital flow around a circular cylinder: Part 2. Attached flow at larger amplitudes. *J. Fluid Mech.* (submitted).

FARADAY, M. 1831 On a peculiar class of acoustical figures; and on certain forms assumed by groups of particles upon vibrating surfaces. *Phil. Trans. R. Soc. Lond.* **121**, 299–340.

HONJI, H. 1981 Streaked flow around an oscillating circular cylinder. *J. Fluid Mech.* **107**, 509–520.

KIM, S. K. & TROESCH, A. W. 1989 Streaming flows generated by high frequency small-amplitude oscillations of arbitrarily shaped cylinders. *Phys. Fluids* A **1**, 975–985.

KUBO, S. & KITANO, Y. 1980 Secondary flow induced by a circular cylinder oscillating in two directions. *J. Phys. Soc. Japan* **49**, 2026–2037.

KUSUKAWA, K., SHIMIZU, Y. & SHINODA, A. 1980 The secondary flow about a circular cylinder oscillating rotationally around an eccentric axis. *J. Phys. Soc. Japan* **49**, 2400–2406.

LONGUET-HIGGINS, M. S. 1970 Steady currents induced by oscillations round islands. *J. Fluid Mech.* **42**, 701–720.

MILNE-THOMSON, L. M. 1968 *Theoretical Hydrodynamics*, 5th edn. Macmillan.

OGILVIE, T. F. 1963 First- and second-order forces on a cylinder submerged under a free surface. *J. Fluid Mech.* **16**, 451–472.

RAYLEIGH, LORD 1883 On the circulation of air in Kundt's tubes and on some allied acoustical phenomena. *Phil. Trans. R. Soc. Lond.*, **175**, 1–21.

RILEY, N. 1971 Stirring of a viscous fluid. *Z. Angew. Math. Phys.* **22**, 645–653.

RILEY, N. 1978 Circular oscillations of a cylinder in a viscous fluid. *Z. Angew. Math. Phys* **29**, 439–449.

SARPKAYA, T. 1986 Force on a circular cylinder in viscous oscillatory flow at low Keulegan–Carpenter numbers. *J. Fluid Mech.* **165**, 61–71.

TANEDA, S. 1980 Visualisation of steady flows induced by a circular cylinder performing a rotary oscillation about an eccentric axis. *J. Phys. Soc. Japan* **49**, 2038–2041.

WANG, J. C. T. & SHEN, S. F. 1978 Unsteady boundary layers with flow reversal and the associated heat-transfer problem. *AIAA J.* **16**, 1025–1029.